Journal of Thermal Analysis and Calorimetry, Vol. 76 (2004) 677–684

EFFECT OF DRYING ON POROUS SILICON

M. Bouchaour[*], *A. Ould-Abbas, N. Diaf and N. Chabane Sari*

Laboratoire de Matériaux et Energies Renouvelables, Université Abou Bakr Belkaid,
B.P: 119 Tlemcen 13000 Algérie

Abstract

The phase transition of a fluid – in particular water – confined in the pores of silicon during drying is studied. The influence of this process on surface size and porosity is discussed. Methods of air drying, supercritical drying and freeze drying are considered.

Keywords: drying, morphology, phase transition, porous silicon

Introduction

Porous silicon (PS) is widely used as an anti-reflection coating, for example, for solar cells [1]. Its porous nature is utilized for surface texturing of single or multi-crystalline Si materials [2]. PS can also act as a surface passivating layer, since it has a larger bandgap than silicon (>1.40 eV). In 1990 Canham observed strong photo-luminescence of PS at wavelengths of visible radiation at room temperature [3]. Because this effect offered miscellaneous applications in optoelectronics, extensive studies of this material were started.

The luminescent properties of PS are sensitive to ambient conditions and the electronic properties at the surface of PS play a key role in obtaining luminescence from this material. When PS is stored or heated in ambient air, the oxidation will break the unstable Si–H bonds at the surface and introduce more Si dangling bonds [4], which decrease luminescent intensity [5].

In order to eliminate or reduce the capillary stress, many methods of drying have been developed. The aim of this paper is to contribute to the understanding of the behaviour of porous silicon during drying. After describing the process of formation of PS we present a short survey on usual drying methods. Then we report studies of the phase transition of a fluid confined in the pores of silicon and analyze the condensation of water in more detail.

Formation of porous silicon

PS was discovered in 1956 by Uhlir while performing electropolishing experiments on silicon wafers using an HF containing electrolyte. He found that on increasing the

* Author for correspondence: E-mail: m_bouchaour@mail.univ-tlemcen.dz

1388–6150/2004/ $ 20.00
© 2004 Akadémiai Kiadó, Budapest
Akadémiai Kiadó, Budapest
Kluwer Academic Publishers, Dordrecht

current over a certain threshold, a partial dissolution of the silicon wafer started to occur. PS formation was then obtained by electrochemical dissolution of Si wafers in aqueous or ethanoic HF solutions [6].

Up to now several different mechanisms regarding the dissolution chemistry of silicon have been proposed, but it is generally accepted that holes are required for both electropolishing and pore formation. The release of hydrogen decreases on approaching the electropolishing regime and stops during the electropolishing. During pore formation, two electrons are used up for each Si atom that reacted and about four electrons are used under electropolishing regime [7]. The overall anodic semi-reactions during pore formation can be written as [8]:

$$Si+6HF \rightarrow H_2SiF_6+H_2+2H^++2e^-$$

and during electropolishing as

$$Si+6HF \rightarrow H_2SiF_6+4H^++4e^-$$

In both cases, the final and stable product for Si in HF is H_2SiF_6, or its ionised forms; it follows that during the pore formation only two of the four available Si electrons participate in an interface charge transfer while the remaining two lead to hydrogen formation. During the electropolishing all four electrons of Si are electrochemically active.

Among the various models proposed for the Si dissolution reaction, the mechanism presented by Lehmann and Gösele (Fig. 1) is the most widely accepted [9]. The mechanism is based on a surface oxidation scheme, with hole capture, and subsequent electron injection, which leads to the Si in divalent state.

According to the model, the Si–H bonds passivate the Si surface unless a hole is available. Once PS is formed, the interpore region is depleted of holes as is evident by the high resistivity of PS ($\approx 10^6$ Ω cm, similar to intrinsic Si). Further dissolution occurs only at the pore tips, where enough holes are available. In this way the etching of PS

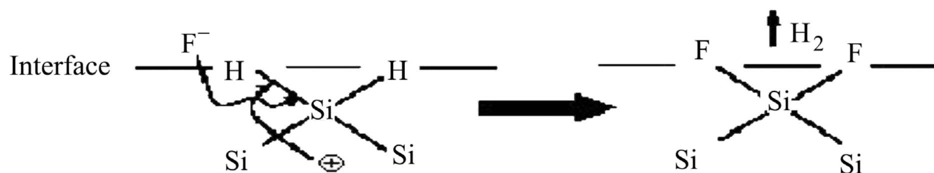

Fig. 1 Hole injection and attack on a Si–H bond by a fluoride ion–silicon dissolution scheme proposed by Lehmann and Gösele

proceeds in depth with an overall directionality which follows the anodic current paths inside Si. Once a PS layer is formed no more electrochemical etching occurs but a slow chemical one starts, due to the permanence presence of the wafer Si in HF [7].

Drying of the samples

An important step in the fabrication process of high quality PS layers is the drying recipe employed immediately after the etching of the wafer. It has been reported several times that the formation of PS, with high porosity (greater than 70%) and/or thickness (of the order of μm) leads to a systematical cracking of the layer during the evaporation of the solvent. A typical example of cracking pattern is reported in Figs 2 and 3 [10]. The origin of the cracking is the large capillary stress associated with evaporation from the pores. During the evaporation a gas/liquid interface forms inside the pores and a pressure drop Δp across the gas/liquid interface occurs. Δp is given by:

$$\Delta p=\gamma\frac{S\cos\Theta}{P} \qquad (1)$$

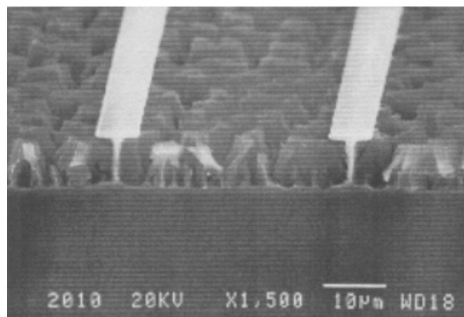

Fig. 2 Cross-sectional SEM image of typical cracking pattern. The white stripes are due to crystalline Si which survives the etching [7]

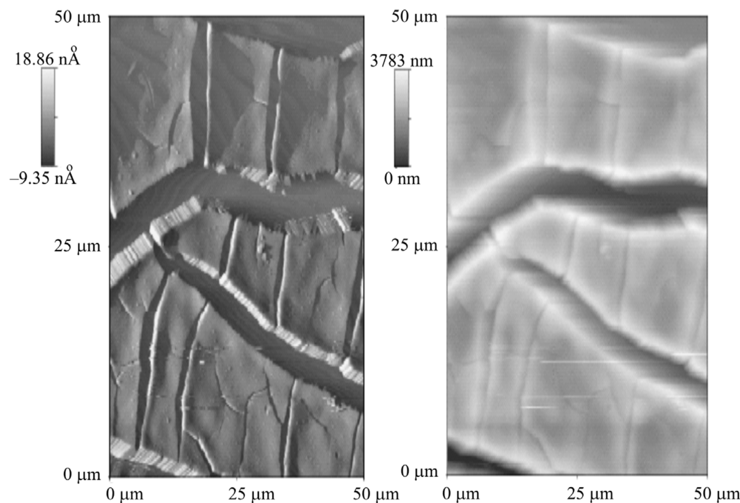

Fig. 3 Cracks in 80% porosity and 3 μm thickness PS layer, after water drying [10]

where γ is the liquid surface tension, S the interface area, $\cos\Theta$ is the curvature of the gas/liquid interface, and P the porosity which is given by [11]:

$$P=\frac{\Delta M}{hS\rho} \tag{2}$$

where S, ρ and h were the anodic etching area of the Si wafer and the density of the Si wafer (i.e., 2.33 g cm^{-3}) and the thickness of the PS film.

Δp values as high as several MPa are measured (Fig. 4) [8].

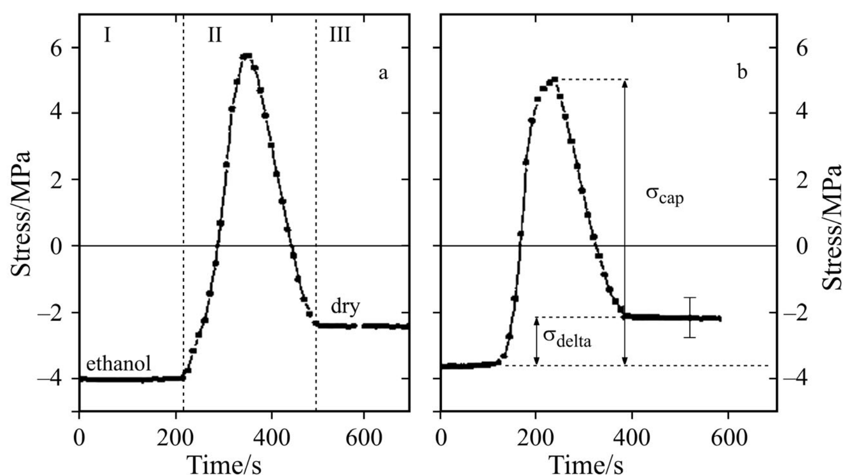

Fig. 4 Stress-time evolution during the drying of PS: a – and b – refer to two cycles

The cracking of highly porous silicon layers during drying can be avoided either by using supercritical drying as shown by Canham *et al*. [12] or by replacing water with another liquid of lower surface tension, like pentane. Freeze drying [13] and slow evaporation rates are also used in the drying of PS to reduce or eliminate the capillary stress.

Pentane drying is the easiest to implement. Pentane has a very low surface tension (i.e. low γ values in Eq. (1)), and shows no chemical interaction with PS (unlike ethanol). Using pentane as rinser, it is possible to reduce strongly the capillary tension; but since water and pentane are non-miscible liquids, ethanol or methanol has to be used as intermediate liquids. Using this drying technique PS layers with porosity values up to 90% and thickness up to 5 μm exhibit no cracking pattern after drying.

Supercritical drying is based on the fact that when the pressure is raised, the interface between the liquid and the gas phase becomes unstable; and when the pressure is larger than the critical pressure, the gas/liquid interface disappears and a mixture of the two phases appears (supercritical fluid). This is the most efficient drying method. In such a technique, the HF solution is replaced by a suitable 'liquid', usually carbon dioxide, under high pressure. The phase is then moved above the critical

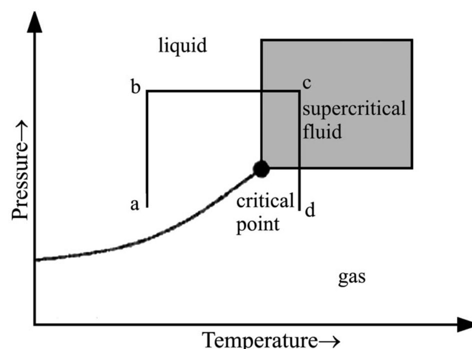

Fig. 5 Schematic phase diagram showing pressure–temperature paths used in supercritical drying

point (31°C) by raising the pressure and temperature, as schematically shown in Fig. 5, path a–b, b–c. Then the gas is removed by the supercritical liquid (Fig. 5, path a–b, c–d). This drying procedure allows production of layers with very high thickness and porosity values (up to 95%), improving the optical flatness and also the homogeneity. However supercritical drying is expensive and complicated to implement so other drying methods are normally employed [8].

The freeze drying process consists of a rapid solidification of the solvent in the pores, obtained by lowering the temperature, T, followed by sublimation under vacuum. This method has been performed on samples etched under certain conditions. The scheme of the process is depicted in Fig. 6. After rinsing the sample in deionised water, the solvent filling the pores is in thermodynamic state A. By decreasing T, the system is brought to the state B by immersing the wet PS sample in liquid nitrogen. This allows solidification of the solvent (mainly water) without any volume expansion, a process obviously harmful for the PS skeleton. The sample is then placed on a cold (~200 K) finger placed in a vacuum chamber. The chamber is evacuated to a pressure P ~0.1 mbar (state C), then the temperature of the cold finger is raised at low rate (0.7 K min^{-1}) to the state D (dried sample). The complete process takes almost 2 h [14].

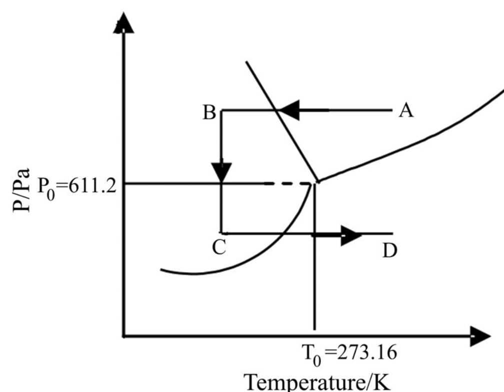

Fig. 6 Schematic diagram of the freeze drying process. In this case the solvent is water

Phase transition of confined materials

In this section, we discuss the phase transition of confined materials and in particular the case of water.

It is well known that the phase transitions of materials confined in small pores are influenced by the effects of curvature, as shown by two typical situations:

- Capillary condensation of a liquid phase in a porous solid occurs at a vapour pressure lower than the saturation pressure of the bulk liquid, and the radius of the meniscus is related to the vapour pressure by the Kelvin equation [15].
- Melting of a confined material occurs generally at a temperature lower than that of bulk melting. Bellet *et al*. [12] consider the ideal case of a liquid in a circular cylinder of radius r with a solid/liquid interface. Then all the interfaces are spherical with radii R_{sl}, related to r by $r=R_{sl}\cos\theta_{lw}$, where θ_{lw} is the contact angle of the liquid with the wall (w) given by the Young equation (3):

$$\gamma_{sl}\cos\theta = \gamma_{sw}-\gamma_{lw} \quad (3)$$

where γ_{sl} is the average isotropic surface energy for the phase system solid–liquid (*s–l*), phase system solid–vapour (*sv*), phase system liquid–vapour (*lv*).

Table 1 presents physical properties of the different fluids used in DSC [16], for the investigation of phase transition in PS according to [17].

Table 1 Physical properties of the different fluids studied by DSC

Liquid	Transition temperature/K	Latent heat of transition. ΔH_{sl}/J g^{-1}	Interfacial free energy γ_{sl}/m J m^{-2}
Cyclo-hexane s–l	279.5	31.9	4.6
s–s	186	79.8	9
Dodecane	263	214	13.5
Water	273	334	25–26

In the case of water, the investigation of the confinement of water in the PS pore network is complicated. but its interest is important. First of all, while PS is often in contact with water (during formation, anodic oxidation, electroluminescence phase, freeze drying, etc.), the interaction between PS and water is not yet fully understood. A direct application of this study is related to the freeze drying of PS filled with water which has been using to avoid the cracking of highly porous silicon layers [13, 14].

Application on p^+ type PS samples

After being detached, the PS layers were oxidized at 300°C in an oxygen atmosphere for one hour. This oxidation allows the internal surface to become hydrophilic. Figure 7a presents the results of the experiment performed on a p^+ type layers of 60% porosity and 100 μm thickness given by Bellet *et al*. [17]. The author noted that after

several scanning cycles, there is still only one single freezing peak. This feature is explained by the large nucleation hysteresis of pure water: when the excess bulk water freezes, the nucleation delay is already more than 14 K, so it induced immediately the freezing of the confined water, thus giving a single freezing peak corresponding to both bulk and confined water freezing. For increasing temperature, the usual behaviour is observed: the confined ice melts first, followed by the melting of bulk extended ice around 272 K. To observe water freezing inside the pores, the heating is stopped just after the complete melting of the confined water (i.e. for a temperature in between the two peaks of the melting DSC curve). Afterwards the temperature was decreased at the same constant scanning rate of 2.5 K min^{-1}, giving the DSC curves presented in Fig. 7b: in such conditions, the excess bulk water does not melt, so that when the temperature is decreased, there is still a frozen bulk water crust outside the sample pore network, and the confined water freezing peak can now be observed. Figure 7b shows a double maximum for the freezing peak as usually observed for this kind of p$^+$ type PS sample. For freezing, the transition temperature shift is ΔT=8.3 and 4.6 K for the double freezing peak, whereas the melting curve exhibits a 3.4 K temperature shift relative to bulk melting T_0.

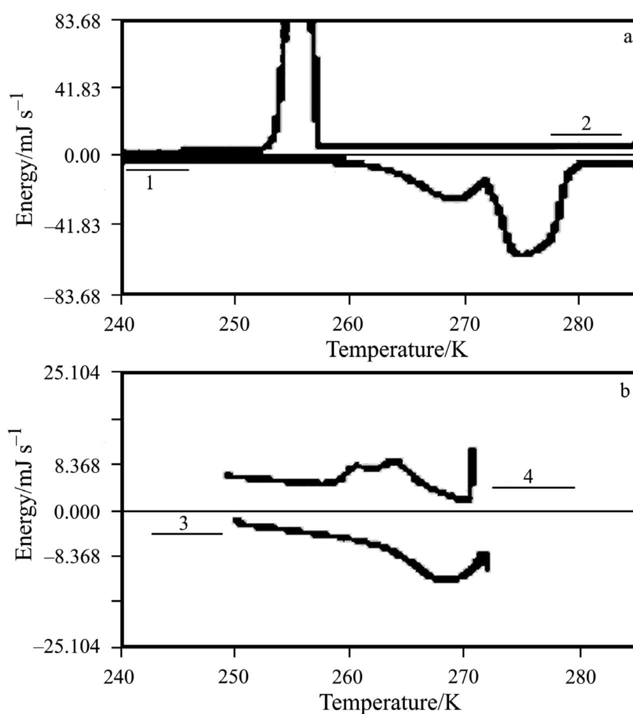

Fig. 7 DSC curves at a scanning rate of 2.5 K min^{-1}, for water confined in a thermally oxidized p$^+$ type PS sample of 60% porosity and 100 μm thickness: a – a full cycle, 1 – increasing and 2 – decreasing temperature, b – for a reduced cycle: 3 – increasing temperature up to 270°C, and then 4 – decreasing temperature

At the end of the experiment, the amount of water involved in the phase transition remains constant after the freezing of water in the pores, proving then that the porous layer does not undergo a cracking phenomenon.

Conclusions

We have described in this paper the effect of confined fluid (water) in the pores of thick p^+ type porous silicon. The formation of PS and methods of drying of this material were also discussed. DSC appears to be a suitable technique for the investigation of inhomogeneity in terms of pore sizes of PS layers, as described by Faivre *et al*. The freeze process appears to be a suitable technique to avoid or reduce the cracking of highly porous materials.

References

1 P. Menna, G. Di Francia and V. La Ferrara, Solar Energy Materials and Solar Cells, 37, pp. 12–24, 1995.
2 R. R. Bilyalov, B. Groh, H. Lautenschlager, R. Schindler and F. Schomann, Proc. of the 26th PVSC, Anaheim, CA, Sept. 30–Oct. 3, pp. 147–150, 1997.
3 L. Canham, Appl. Phys. Lett., 57 (1990) 1041.
4 M. A. Lieberman and A. J. Lichtenberg, John Wiley & Sons Inc., New York 1994.
5 D. Zhu, Q. Chen and Y. Zhang, J. Lumin. Porous Silicon, 0, 1–5, 2002.
6 V. Lehman and U. Gösele, Appl. Phys. Lett., 58 (1991) 856.
7 C. Vinegoni, M. Cazzanelli and L Pavesi, Manuscript redacted at University of Pittsburgh, USA, October, 2000.
8 O. Bisi, S. Ossicini and I. Pavesi, Elsevier Surface Science Reports, 38 (2000) 1.
9 P. Roussel, Thèse de Doctorat, Lyon 1999.
10 I. Kleps and A. Angelescu, Romanian J. Inf. Sci. Tech., 1 (1998) 167.
11 Q. Shen and T. Toyoda, J. Therm. Anal. Cal., 69 (2002) 1067.
12 D. Bellet and L. Canham, Adv. Mater., 10 (1998).
13 G. Amato and N. Brunetto, Mater. Lett., 26 (1996) 295.
14 G. Amato, N. Brunetto and A. Parisini, Thin Solid Films, 297 (1997) 73.
15 R. Defay, I. Prigogine, A. Bellemans and D. H. Everett, Longmans, Green and Co., London 1966.
16 A. Książczak, A. Radomski and T. Zielenkiewicz, J. Therm. Anal. Cal., 74 (2003) 559.
17 C. Faivre, D. Bellet and G. Dolino, Eur. Phys. J. B 7, 19–36, 1999.